




Synthesis and structural characterization of MoS₂ micropyramids

J. Enrique Samaniego-Benitez^{1,*} , Rubén Mendoza-Cruz², Lourdes Bazán-Díaz², Alejandra Garcia-Garcia³, M. Josefina Arellano-Jimenez⁴, J. Francisco Perez-Robles⁵, German Plascencia-Villa⁶, J. Jesus Velázquez-Salazar⁶, Eduardo Ortega⁷, Sarai E. Favela-Camacho⁸, and Miguel José-Yacamán⁹

¹ Catedras Conacyt, Instituto Politécnico Nacional, CICATA Unidad Legaria, 11500 Ciudad de México, Mexico

² Instituto de Investigaciones en Materiales, Universidad Nacional Autónoma de México, 04510 Ciudad de Mexico, Mexico

³ Laboratory of Synthesis and Modification of Nanostructures and Bidimensional Materials, Centro de Investigación en Materiales Avanzados Unidad Monterrey, 66628 Monterrey, Nuevo Leon, Mexico

⁴ Department of Materials Science and Engineering, The University of Texas at Dallas, Richardson, TX 75080, USA

⁵ Centro de Investigación y de Estudios Avanzados del I.P.N. Unidad Querétaro, 76230 Querétaro, Querétaro, Mexico

⁶ Department of Physics & Astronomy, The University of Texas at San Antonio, San Antonio, TX 78249, USA

⁷ INM- Leibniz Institute for New Materials, 66123 Saarbrücken, Germany

⁸ Universidad Tecnológica de Manzanillo, 28869 Manzanillo, Colima, Mexico

⁹ Department of Applied Physics and Materials Science, Center for Materials Interfaces Research and Applications (MIRA), Northern Arizona University, Flagstaff, AZ 86011, USA

Received: 5 December 2019

Accepted: 26 May 2020

Published online:
4 June 2020

© Springer Science+Business Media, LLC, part of Springer Nature 2020

ABSTRACT

Two-dimensional (2D) materials based on molybdenum sulfide (MoS₂) have shown promising applications in semiconductors, optoelectronics, and catalysis. The variety of applications implies a controlled manipulation of purity, shape, and phase of such materials. This work elaborates on the structural characterization of MoS₂ micro-assemblies produced in a chemical vapor deposition (CVD) system with emphasis on the pyramidal structures formed at high temperature and low gas rate, on a silicon dioxide (SiO₂) substrate. A precise control of temperature and gas rate in the CVD process prompts the growth of pyramidal and other micron-size arrangements of MoS₂ layers. An integrative set of high-resolution and analytical electron microscopy techniques, in conjunction with Raman and X-ray photoelectron spectroscopy (XPS), revealed the structural features of the MoS₂ microstructures. Raman and XPS confirmed the presence of MoS₂ and some residual oxide phases. Ultra-high-resolution scanning electron microscopy provided direct observation of the distinctive stacking of layers forming the pyramidal microstructures. Cross section samples from selected structures were done using focused ion beam. An extent of transmission electron microscopy and Cs-corrected scanning transmission electron microscopy (Cs-corrected STEM) results is discussed. This approach allowed to

Address correspondence to E-mail: enriquesabe1809@gmail.com

understand the growth mechanism of the triangular MoS₂ microstructures through spiral grow around a screw dislocation, initiated at the center of the assembly.

Introduction

Two-dimensional (2D) transition metal dichalcogenides (TMDs) are a versatile family of nanomaterials with more than forty layered composites. They have the general formula MX₂, where M is a transition metal of the groups 4–10 of the periodic table, and X is the respective chalcogen [1–4]. Molybdenum (IV) disulfide (MoS₂) is one in this type of 2D layered materials that come up with a variety of promising applications in nanoelectronics, photonics, sensing, energy storage, and optoelectronics [3, 5–8]. For instance, MoS₂ exhibits weak interlayer Van der Waals interactions that allow it to act as an efficient host for a variety of electron donating atoms, such as lithium or sodium, to produce nano-batteries [9]. In bulk, MoS₂ exhibits a semiconductor behavior with an indirect bandgap of 1.29 eV, but it drastically differs when becomes a monolayer, having a transition to a direct bandgap of around 1.8 eV [8, 10]. The displayed properties are directly related to its crystalline structure and particular three-dimensional arrangement. One of the biggest challenges in the synthesis of MoS₂ materials is advancing reliable methods to produce specific nanometric-size arrangements and fine tune their properties. Among the different methods employed to modify and control the structural properties of MoS₂ are: mechanical synthesis [11], wet chemistry [12], exfoliation [13], and chemical vapor deposition (CVD) [14]. CVD is particularly useful for large-scale production of 2D MoS₂, enabling direct growth of materials over-activated solid substrates using gas-phase precursors. An efficient control of the reaction conditions allows the production of uniform thin layers [15], or vertically aligned MoS₂ films [16]. Moreover, this method enables the overall shape control of deposited layers, using elemental molybdenum and sulfur as precursors, to produce high-quality single-layer MoS₂ thin flakes, with triangular and hexagonal shapes, extended on solid substrates [17, 18]. Shape and structure effect the properties and consequently the applications of multilayered materials; e.g., a preferred pyramidal arrangement of layers exposes a

succession of edges over the pyramidal steps which have potential catalytic applications [19–22]. Hence, the detailed study of morphological and structural features of 2D materials becomes of paramount importance to understand their evolution and properties.

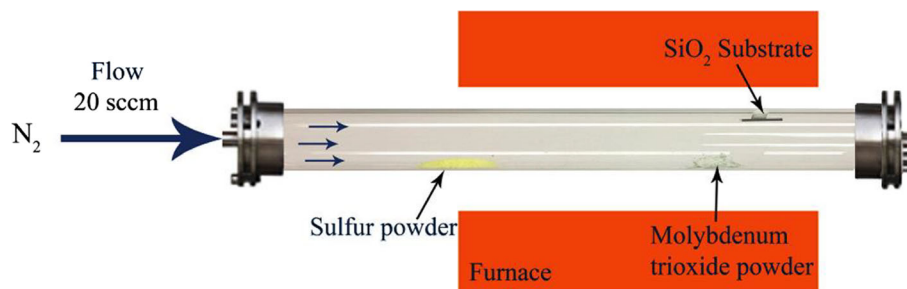
Previous reports described the growth of 2D MoS₂ as a screw-dislocation-driven process [23–29], and the study of layered microstructures has been conducted using atomic force microscopy (AFM) and Raman spectroscopy. Typically, MoS₂ exhibits a centrosymmetric 2H-hexagonal phase described by an ABAB stacking of S–Mo–S layers, with coplanar S–Mo–S atoms in the first layer opposite to the second layer. However, other non-centrosymmetric phases have been reported specially when dealing with few layered materials and screw-dislocation pyramidal morphologies [24, 25, 30, 31]. In this work, pyramidal microstructures made of MoS₂ were produced in a CVD system. Their structural characteristics were investigated using spectroscopy and electron microscopy techniques, namely Raman, X-ray photoelectron spectroscopy (XPS), ultra-high-resolution scanning electron microscopy (UHR-SEM), focused ion beam (FIB), and transmission electron microscopy (TEM). Emphasis placed on the structural characteristics is aimed to expand the understanding on the growth of MoS₂ microstructures.

Experimental section

Synthesis

MoS₂ microstructures were synthesized via CVD, protocol adapted from Chen et al. [24]. The experiment setup is illustrated in Fig. 1. A 5 × 5 mm section of ultra-flat [100] SiO₂ wafer was used as a substrate for the preferential growth of MoS₂. The SiO₂ piece was previously cleaned using an isopropyl alcohol/acetone (1:1 volume) solution. In a typical growth reaction, 0.3 g of molybdenum trioxide (MoO₃) powder (99%, Sigma-Aldrich) was placed in an alumina boat located at the center of a quartz tube

Figure 1 The schematic shows the location of substrate and precursor materials in the CVD system used for the growth of MoS₂ pyramids.



(2.5 cm in diameter and 60 cm long). The boat position was at the center of the heating zone of the furnace (Lindberg Blue STF55433). Next, 0.6 g of sulfur powder (99% Sigma-Aldrich) was placed in the inlet of the furnace 15 cm away from the center. During a typical procedure, the furnace temperature was set to 900 °C following a linear ramp of 10 °C min⁻¹ under a 20 sccm flow of N₂ gas. The system was maintained during 20 min at 900 °C, time in which the sulfur evaporated entirely and reached the center of the reactor to interact with the MoO₃ [32, 33]. Finally, the system was cooled down to room temperature under N₂ atmosphere.

Characterization

Raman spectroscopy studies were performed with a LabRam HR Evolution from Horiba at ambient conditions with controlled light and a back-scattering configuration at a wavelength of 633 nm laser. For mapping, an acquisition time of 5 s and 10 accumulations were used for each point with a grid of 10 × 10, an objective lens of 100× Vis and grating of 500 nm. X-ray photoelectron spectroscopy (XPS) spectra were obtained in an ESCALAB 250Xi (Thermo Scientific) X-ray photoelectron spectroscope using monochromatic AlK α radiation ($h\nu = 1486.7$ eV). Images of the surface morphology of the MoS₂ pyramids were acquired with an opto-digital microscope (Olympus DSX500), an ultra-high-resolution field-emission scanning electron microscope (UHR FE-SEM Hitachi 5500), and with a FIB-scanning electron microscope (FIB-SEM, ZEISS Crossbeam 340). A cross section of the pyramidal structure was obtained through FIB microsectioning using Ga ions at 30, 5, and 2 kV. The pyramid was previously coated with a layer of carbon and platinum to protect the sample from gallium ions. Plain-view imaging of the microstructure was performed with a high-resolution transmission electron microscope (HRTEM,

JEOL 2010F). Experimental HRTEM images are compared with a simulated 2H.MoS₂ structure generated by SimulaTEM software [34]. Atomic resolution imaging was carried out in a Cs-corrected transmission electron microscope (JEOL ARM-200F) operated in scanning mode (STEM) at 200 kV.

Results and discussion

The SiO₂ substrate was explored through optical microscopy to determine the structures obtained through the CVD process (Fig. 2). It is possible to observe pyramidal microstructures obtained through the CVD process in the images of bright-field (2a–b) and dark-field (2c–d) mode, such structures are indicated with arrows.

The deposit of MoS₂ on the SiO₂ substrate as a result of the CVD process was observed with more detail through SEM imaging, Fig. 3. It's noticed the formation of an irregular film (or “islands”) on the substrate, Fig. 3a. At the edge of this irregular film, it

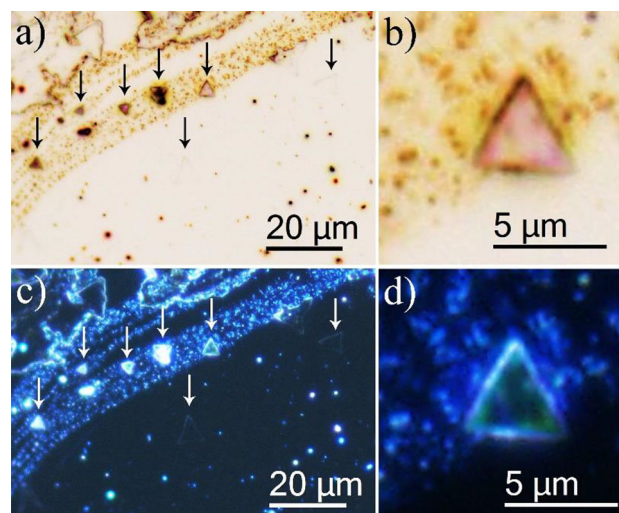


Figure 2 Bright-field (a, b) and selected area dark-field optical images (c, d) of the SiO₂ piece after the CVD process.

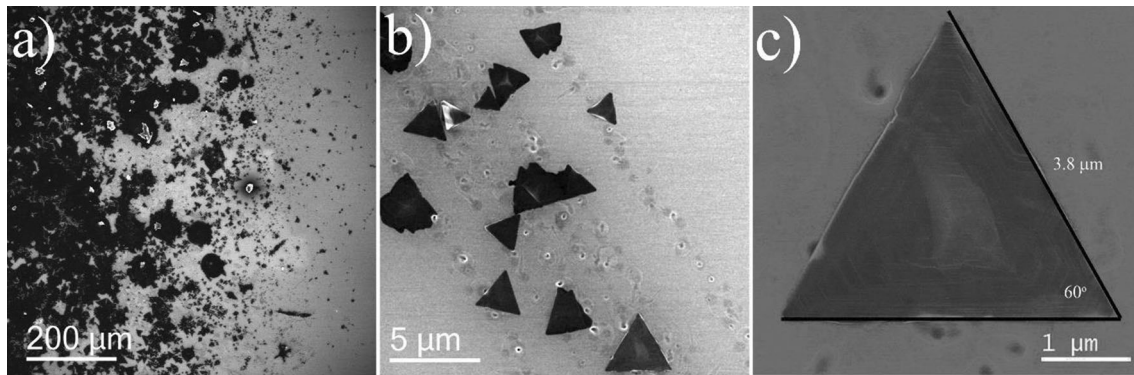


Figure 3 a SEM images of the “islands” and b and c pyramidal structures of MoS₂ at different magnifications.

is possible to observe the abundant formation of triangular structures, with some degree of truncation or shape irregularity (Fig. 3b). Some of these microstructures present a perfect triangular shape, such as the one shown in Fig. 3c, with a size of 3.8 μm per side, where the stepped surface is visible.

The Raman spectrum of the micropylamid are shown in Fig. 4, where the color of each spectrum corresponds to the color assigned to each circle shown in the mapped area. Mapping analysis revealed the appearance of characteristic MoS₂ signals at 179 (A_{1g}(M) – LA(M)), 230 (LA(M)), 383 (E_{2g}¹), 409 (A_{1g}), 421 (B_{2g}² + E_{1u}²), 454 (2LA), and 465 cm⁻¹ (A_{2u}) [35–37] corresponding to the spectra of the shown areas. However, there are some differences between the spectrum obtained from the central area of the micropylamid (red spectrum or

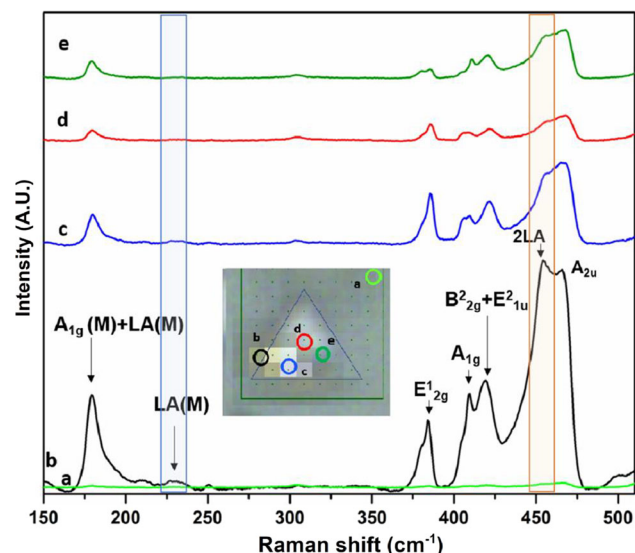


Figure 4 Raman spectra of different points on the MoS₂ pyramids grown by CVD (633 nm laser).

labeled with the letter d) and the spectrum obtained on the edge labeled with the letter b, black circle. The spectrum obtained from the central area shows a value of the I_{2LA(M)}/I_{A_{2u}} ratio of 0.98, while the I_{2LA(M)}/I_{A_{2u}} ratio for the black spectrum was 1.05, which indicates that the 2LA(M) mode shows a high value of intensity at the edge of the micro pyramid. According to Chakraborty et al. [36], the relative intensity of the 2LA(M) mode respect to the A_{2u} mode decreases as a function of the number of layers, correlating with our results since at the center of the micropylamid the number of layers is greater than in the edge. The relationship between the 2LA(M) and A_{2u} modes for the spectra c and e indicates a 2H-type structure similar to the to the bulk material, while in the a spectrum the presence of MoS₂ is null since the mapping was carried out outside the micropylamid. Another vibrational mode observed in the spectrum and taken at the edge of the micropylamid is located at 230 cm⁻¹ (mode LA(M)) taken at the edge of the micropylamid. This mode is identified as first-order mode, and it is attributed to the dispersion of phonons due to defects induced in the structure and the presence of a few atomic layers. Finally, a slight signal was also observed around 300 cm⁻¹, which may be due to the presence of molybdenum oxides remaining from the synthesis [38–40].

The XPS analysis of the MoS₂ pyramids is displayed in Fig. 5. In the high-resolution spectrum of the S2p region (Fig. 5a), the 2p_{1/2} and 2p_{3/2} signals of the MoS₂ are observed at 163.1 and 161.8 eV. Also, two signals are observed at 162.4 and 161.3 eV, which can be assigned to non-stoichiometric Mo_xS_y due to the presence of surface defects introduced during the CVD growth [41, 42]. The S2s-Mo3d region is displayed in Fig. 5b. The S2s (226.50 eV) and Mo 3d

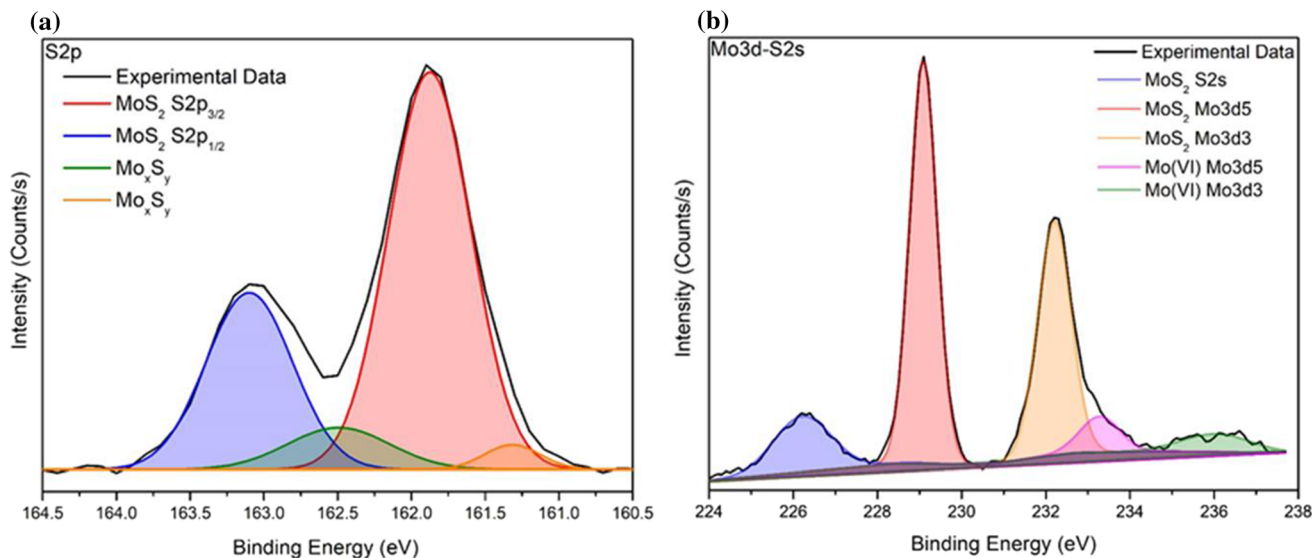


Figure 5 High-resolution XPS spectrum of S2p **a** and S2s-Mo3d **b** regions of the MoS₂ micropyramids.

(229.1 and 232.2 eV for 3d_{5/2} and 3d_{3/2}, respectively) correspond to signals of MoS₂ are observed [43–45]. Other signals located at 233.3 eV and 236 eV, are observed, assigned to the 3d_{5/2} and 3d_{3/2} of the Mo(VI) species [46–48]. These results show that the obtained microstructures are almost entirely composed of MoS₂; however, some molybdenum oxide and non-stoichiometric Mo_xS_y phases presented.

A more detailed morphological analysis was carried out by SEM tilting the sample up to 54°, which allows the observation of a distinguishable stepped surface of the micropyramids. The pyramid has a triangular base consisting of several layers of MoS₂. The pyramids correspond to a truncated trigonal morphology with a high density of surface steps, which can be correlated to the speed of growth in the direction of the [0001] axis. It slightly varies since each step has a different number of layers. The obtained pyramidal morphology is related to screw dislocations occurring during the growth of the nucleus along the vertical axis, and to the triangular-shaped layers in the lateral dimension that form the MoS₂ pyramid. A spiral structure of MoS₂ pyramids can be clearly seen, and the direction of growth that occurred in a clockwise direction is indicated with white arrows in Fig. 6a. A schematic of the MoS₂ pyramid growth with a spiral structure is shown in Fig. 6b. The different steps that are formed during the growth of the pyramid are clearly observed in Fig. 6c. The image shows defects at the edges, which cause deviation from the perfect triangular shape. The

combination of morphological features between hexagonal and triangular shapes in the microstructures is due to a complex growth that includes two dislocations that share a common core [29]. In some of the MoS₂ pyramids, we observed the formation of small particles at the edges of the layers and some larger particles dispersed throughout the pyramid. These round particles corresponded to nucleation points for the growth of monolayers of MoS₂ [14]. These images help to understand the growth mechanism of the triangular crystallites. The growth proceeded along emerging screw dislocation on the surface, as demonstrated by the Burton, Cabrera, and Frank theory (BCF) [49, 50]. This type of growth mechanism has been reported in other nanomaterials such as cobalt, nickel hydroxide, zinc hydroxy sulfate, and other pure metals [51–54]. The formation of a screw dislocation in MoS₂ requires the generation of slipped planes (screw defects) in the first layers of the pyramid; otherwise, the growth will preferentially follow an in-plane growth mode, producing monolayers of MoS₂ [25, 55]. Screw dislocations developed under low supersaturation conditions created staggered edges in the bottom layer that act as nucleation sites for the addition of the following precursor atoms, driving the growth of the second layer in the top of the bottom layer. This gradually leads to the continuous growth of spirals, resulting in a pyramidal growth [50]. These conditions of low-saturation conditions were reached in our experiment set up by the low sulfur concentration present at the center of

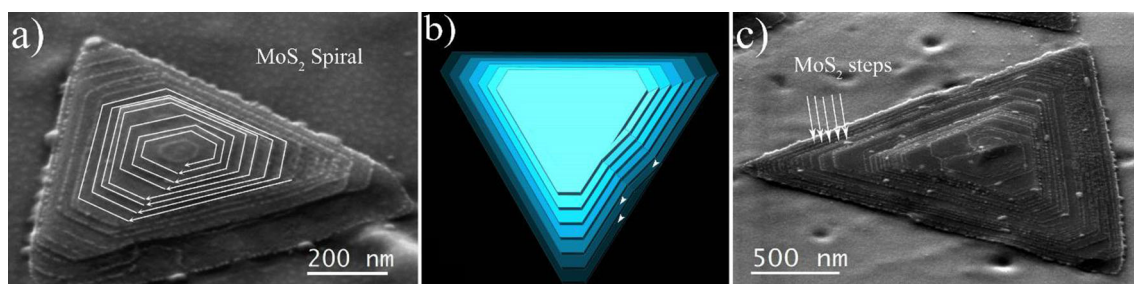


Figure 6 **a** SEM image of MoS₂ pyramid showing the spiral growth mechanism. **b** Schematic model of the MoS₂ pyramid. **c** SEM image of a MoS₂ pyramid is showing the multiple layered steps.

the reactor and by controlling the low drag flow velocity. For most of the reported experiments for the growth of MoS₂ using CVD the rate of the carrier gas is usually high, ranging from 100 to 500 sccm [14, 56, 57], in comparison with our process at only 20 sccm.

Dichalcogenide MoS₂ present typically a 2H-hexagonal phase with an ABAB stacking. This stacking order can vary depending on the morphology, thickness, growth mechanism, etc. [24, 25, 31, 58]. To confirm the structural arrangement of the produced MoS₂ pyramids, HRTEM and atomic-resolution STEM imaging were performed. First, complete structures were recovered by scraping the surface of the SiO₂ substrate with a thin blade, then placed into an ethanol solution and resuspended with an ultrasonic bath for 20 min. Afterward, 7 μL of the ethanol solution was placed onto a carbon-coated TEM grid, and the solvent was allowed to evaporate at room temperature. A second sample was prepared by FIB cross-sectioning, attaching the fabricated lamella on a copper lift-out grid. Figure 7a (scraped sample) shows an HR-TEM micrograph of a scraped MoS₂ pyramid, confirming the crystalline arrangement achieved during the CVD production process. No perceivable defects were found in the analyzed areas. The three interplanar distances were 0.27 nm, with 60° between them. These distances matched with the (0 $\bar{1}$ 10), (1 $\bar{1}$ 00), and (10 $\bar{1}$ 0) planes of the 2H-MoS₂ structure, viewed along the [0001] direction. The corresponding electron diffraction pattern is shown in Fig. 7b. The pattern shows sharp reflections characteristic of 2H-MoS₂. Satellite reflections following the hexagonal symmetry of the pattern are also observed, indicating a rotation of ~ 2.6° of some layers around the [0001] axis due to the spiral growth. Micrographs of the pyramid cross section, Fig. 7c, exhibit an area with a periodicity of layers or steps

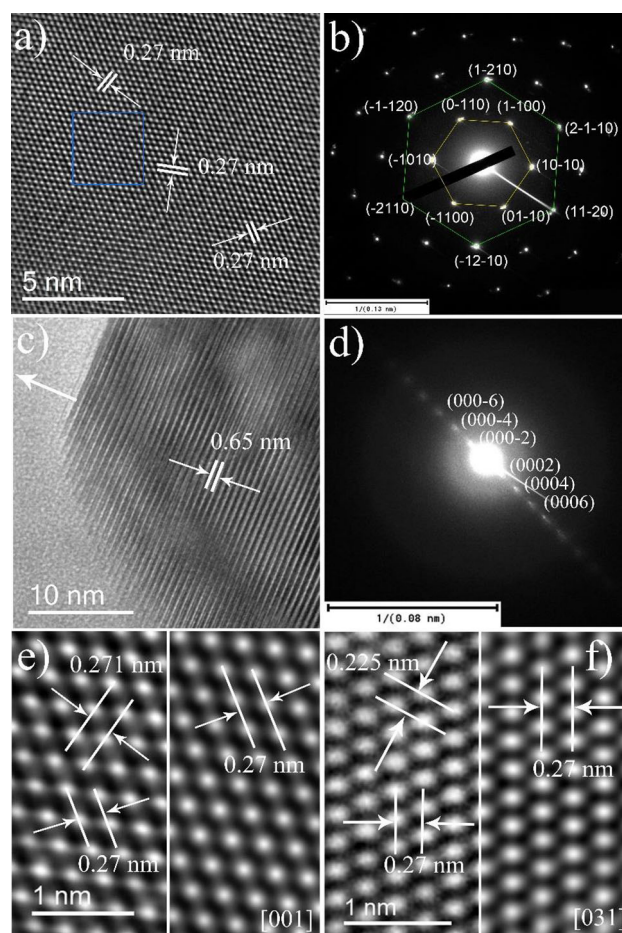


Figure 7 **a** TEM image of MoS₂ pyramid viewed from different zone axis **b** electron diffraction pattern of MoS₂ pyramid viewed from [0001] direction. **c** Cross section area and **d** electron diffraction pattern of the pyramid and composed of 68 layers, their evenly space of 0.65 nm which correspond to the (0002) planes of MoS₂. **e**, **f** Experimental (left) and simulated (right) HRTEM images of a small area of the single pyramid. The lattice pattern is in agreement with a 2H-ABAB layer stacking.

forming the pyramidal arrangement. The overall imaged area was approximately 1 μm², and it is composed of about 68 layers. The interlayer distance

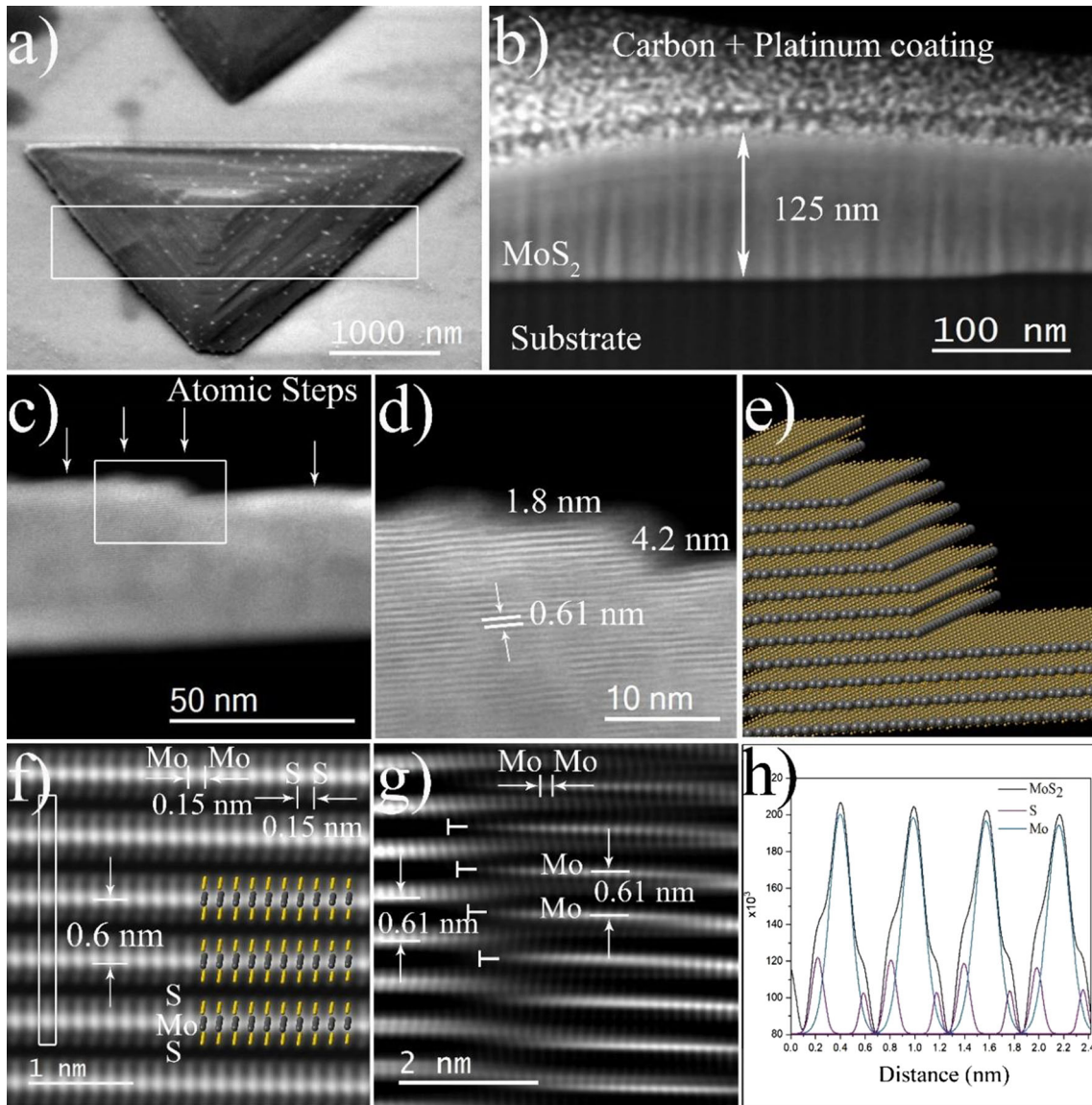


Figure 8 **a** TEM image of the MoS₂ pyramid with a white rectangle where the cross section cut was made. **b** SEM image of cross section obtained using the FIB-SEM. **c**, **d** Aberration-corrected STEM imaging showing the position and height of the atomic steps and separation between the MoS₂ layers **e** atomic model of the MoS₂ structure showing the steps. **f** Atomic

is 0.6 nm, corresponding to {0001} planes. The electron diffraction pattern of the MoS₂ (Fig. 7c, up inset) confirmed the [0001] growth direction. A magnified area of the image indicated with the blue square in Fig. 7a is presented in the left panel in Fig. 7e highlighting the lattice pattern. An HRTEM image of a MoS₂ flake with 2H-ABAB structure viewed from the [0001] axis zone was simulated, right panel in Fig. 6e, taking into consideration the experimental

resolution imaging of the lattice of a MoS₂ with the superimposed model of the structure. **g** Atomic resolution imaging of the layer stacking of MoS₂. **h** Deconvolution of a line profile spectrum of MoS₂ (black line) with peak overlaps of Mo (Blue line), and S (purple line) elements, taken from figure (f).

acquisition conditions. By tilting the sample around the [10 $\bar{1}$ 0] axis, a second HRTEM image was taken along the [03 $\bar{3}$ 1] axis zone, and its corresponding simulated image is also shown, right panel in Fig. 7f. As noticed, the simulated images are in good agreement with the observed experimental lattice patterns along two different axis zones.

Aberration-corrected HAADF-STEM imaging was employed to get a deeper insight into the pyramid's.

Figure 8a shows a MoS₂ pyramid coated with a layer of carbon and platinum to protect it before sectioning. The prepared pyramid's cross section is observed in Fig. 8b. This process enabled to determine that the sample height was of approximately 125 nm close to its center with ~ 200 monolayers of MoS₂, offering a considerable amount of chemically active reactive sites for efficient catalytic applications or to act as support for other functional nanostructured materials. The cross section view revealed four steps clearly defined, the height of each step depending on the number of layers of MoS₂ conforming them (Fig. 8c). In the analyzed area, each step was formed by 3 to 7 layers, which corresponded to a size of 1.8 and 4.2 nm, respectively (Fig. 8d). A schematic of the pyramid showing the different number of layers in each step is presented in Fig. 8e. The cross-sectional atomic-resolution HAADF-STEM image in Fig. 8f enables direct visualization of the stacking order of the pyramid layers. The brightest atomic columns correspond to projected Mo atomic columns, while the dim ones are exclusively S columns. An atomistic model is inserted in the image for comparison. This arrangement corresponds to an ABAB stacking of MoS₂ layers, characteristic of the 2H phase, viewed along the $[1\bar{1}00]$ direction. An atomistic model is inserted in the image for comparison.

An intercalated stacking of MoS₂ originated by the screw dislocation closer to the center of the pyramid is observed in Fig. 8g. It is noted that the ABAB stacking order is retained with very small deviations due to layers deformation or rotation, which can cause the satellite reflections observed in the diffraction pattern in Fig. 6b. The nucleation at the initial stage generates a dislocation center with high spiral activity, which allows maintaining the screw dislocation in the MoS₂ layers. A deconvoluted intensity profile of the selected area shown in Fig. 8f highlights the location of heavy atomic columns (Mo) and light atomic columns (S) throughout the line profile (Fig. 8h). Interplanar distances of 0.6 nm and 0.15 nm were measured, corresponding to interlayer Mo-Mo columns and in-plane Mo-Mo columns, respectively. The difference in the intensities of the S columns in the profile is due to a slight deviation of the sample from the exact axis zone. These cross-sectional images present a direct observation of the MoS₂ layer intercalation produced by the screw-dislocation-driven growth and confirm the 2H-ABAB

stacking order of the produced pyramids in agreement with spectroscopy results [29].

Conclusions

MoS₂ micropyramids were produced by using a CVD growth method using at high temperatures and low gas rates. Raman spectroscopy demonstrated the characteristics signals of MoS₂ on the SiO₂ substrate and highlighted the differences between the vibrational modes at the center and in the edge of pyramids. Signals at 230 and 454 cm⁻¹ attributed to few layers MoS₂ were located at the edge of the pyramids suggesting a one-step formation, while at the center, the signal corresponds to the bulk material. XPS confirmed the presence of the MoS₂ phase in its majority, however, the presence of the Mo (VI) signals are also observed attributed to the presence of an oxide phase. UHR-SEM imaging revealed the preferential formation of pyramidal structures ranging in size between 1 and 4 μm per side. In combination with FIB-SEM, it was possible to determine that the growth mechanism of these materials is dominated by a spiral growth at screw dislocations, particularly due to the low concentration of the sulfur used during the optimized process. Cross sections of MoS₂ pyramids obtained by FIB allowed to reveal the internal arrangement of the materials. In combination with atomic resolution, S/TEM imaging allowed the direct determination of the 2H-ABAB structural stacking along the $[0001]$ direction of the produced pyramids, with horizontal growth along the $[10\bar{1}0]$ and $[0\bar{1}10]$ directions. The high contrast and resolution of the HAADF signal undoubtedly showed the precise organization of MoS₂ into defined atomic steps of S-Mo-S, and the intercalation of layers one by one originated by the screw-dislocation-driven growth.

Acknowledgements

The authors thank CONACyT-Mexico for the support. To Alejandro Arizpe Zapata and Luis Gerardo Silva Vidaurri for technical support at CIMAV Monterrey to perform Raman and XPS measurements and E. Arzt for support through the INM. Enrique Samaniego-Benitez thanks Cátedras Research Program of CONACyT.

References

- [1] Wang QH, Kalantar-Zadeh K, Kis A et al (2012) Electronics and optoelectronics of two-dimensional transition metal dichalcogenides. *Nat Nanotechnol* 7:699–712. <https://doi.org/10.1038/nnano.2012.193>
- [2] Saldanha PL, Brescia R, Prato M et al (2014) Generalized one-pot synthesis of copper sulfide, selenide-sulfide, and telluride-sulfide nanoparticles. *Chem Mater* 26:1442–1449. <https://doi.org/10.1021/cm4035598>
- [3] Haque F, Daeneke T, Kalantar-zadeh K, Ou JZ (2018) Two-dimensional transition metal oxide and chalcogenide-based photocatalysts. *Nano-Micro Lett* 10:1–27. <https://doi.org/10.1007/s40820-017-0176-y>
- [4] McGarrigle EM, Myers EL, Olla O et al (2007) Chalcogenides as organocatalysts. *Chem Rev* 107:5841–5883
- [5] Dai X, Du K, Li Z et al (2015) Enhanced hydrogen evolution reaction on few-layer MoS₂ nanosheets-coated functionalized carbon nanotubes. *Int J Hydrog Energy* 40:8877–8888
- [6] Hinnemann B, Moses PG, Bonde J et al (2005) Biomimetic hydrogen evolution: MoS₂ nanoparticles as catalyst for hydrogen evolution. *J Am Chem Soc* 127:5308–5309. <https://doi.org/10.1021/ja0504690>
- [7] Rowley-Neale SJ, Brownson DAC, Smith GC et al (2015) 2D nanosheet molybdenum disulfide (MoS₂) modified electrodes explored towards the hydrogen evolution reaction. *Nanoscale* 7:18152–18168. <https://doi.org/10.1039/C5NR05164A>
- [8] Ganatra R, Zhang Q (2014) Few-layer MoS₂: a promising layered semiconductor. *ACS Nano* 8:4074–4099. <https://doi.org/10.1021/nn405938z>
- [9] Ramakrishna Matte HSS, Gomathi A, Manna AK et al (2010) MoS₂ and WS₂ analogues of graphene. *Angew Chem Int Ed* 49:4059–4062. <https://doi.org/10.1002/anie.201000009>
- [10] Mak KF, Lee C, Hone J et al (2010) Atomically thin MoS₂: a new direct-gap semiconductor. *Phys Rev Lett* 105:2–5. <https://doi.org/10.1103/PhysRevLett.105.136805>
- [11] Novoselov KS, Jiang D, Schedin F et al (2005) Two-dimensional atomic crystals. *Proc Natl Acad Sci USA* 102:10451–10453. <https://doi.org/10.1073/pnas.0502848102>
- [12] O'Neill A, Khan U, Coleman JN (2012) Preparation of high concentration dispersions of exfoliated MoS₂ with increased flake size. *Chem Mater* 24:2414–2421. <https://doi.org/10.1021/cm301515z>
- [13] Eda G, Yamaguchi H, Voiry D et al (2011) Photoluminescence from chemically exfoliated MoS₂. *Nano Lett* 11:5111–5116. <https://doi.org/10.1021/nl201874w>
- [14] Najmaei S, Liu Z, Zhou W et al (2013) Vapour phase growth and grain boundary structure of molybdenum disulfide atomic layers. *Nat Mater* 12:754–759. <https://doi.org/10.1038/nmat3673>
- [15] Lee Y, Lee J, Bark H et al (2014) Synthesis of wafer-scale uniform molybdenum disulfide films with control over the layer number using a gas phase sulfur precursor. *Nanoscale* 6:2821–2826. <https://doi.org/10.1039/c3nr05993f>
- [16] Kong D, Wang H, Cha JJ et al (2013) Synthesis of MoS₂ and MoSe₂ films with vertically aligned layers. *Nano Lett* 13:1341–1347. <https://doi.org/10.1021/nl400258t>
- [17] Kim D, Sun D, Lu W et al (2011) Toward the growth of an aligned single-layer MoS₂ film. *Langmuir* 27:11650–11653. <https://doi.org/10.1021/la201878f>
- [18] Wu S, Huang C, Aivazian G et al (2013) Vapor-solid growth of high optical quality MoS₂ monolayers with near-unity valley polarization. *ACS Nano* 7:2768–2772. <https://doi.org/10.1021/nn4002038>
- [19] Dong H, Liu C, Ye H et al (2015) Three-dimensional nitrogen-doped graphene supported molybdenum disulfide nanoparticles as an advanced catalyst for hydrogen evolution reaction. *Sci Rep* 5:2–11. <https://doi.org/10.1038/srep17542>
- [20] Daage M (1994) Structure-function relations in molybdenum sulfide catalysts: the “rim-edge” model. *J Catal* 149:414–427
- [21] Tye CT, Smith KJ (2006) Catalytic activity of exfoliated MoS₂ in hydrodesulfurization, hydrodenitrogenation and hydrogenation reactions. *Top Catal* 37:129–135. <https://doi.org/10.1007/s11244-006-0014-9>
- [22] Xie J, Zhang J, Li S et al (2013) Controllable disorder engineering in oxygen-incorporated MoS₂ ultrathin nanosheets for efficient hydrogen evolution. *J Am Chem Soc* 135:17881–17888. <https://doi.org/10.1021/ja408329q>
- [23] Sarma PV, Patil PD, Barman PK et al (2015) Controllable growth of few-layer spiral WS₂. *RSC Adv* 6:376–382. <https://doi.org/10.1039/c5ra23020a>
- [24] Chen L, Liu B, Abbas AN et al (2014) Screw-dislocation-driven growth of two-dimensional few-layer and pyramid-like WSe₂ by sulfur-assisted chemical vapor deposition. *ACS Nano* 8:11543–11551. <https://doi.org/10.1021/nn504775f>
- [25] Zhang L, Liu K, Wong AB et al (2014) Three-dimensional spirals of atomic layered MoS₂. *Nano Lett* 14:6418–6423. <https://doi.org/10.1021/nl502961e>
- [26] Nie Y, Barton AT, Addou R et al (2018) Dislocation driven spiral and non-spiral growth in layered chalcogenides. *Nanoscale* 10:15023–15034. <https://doi.org/10.1039/c8nr02280a>
- [27] Guo Y, Fu X, Peng Z (2018) Controllable synthesis of MoS₂ nanostructures from monolayer flakes, few-layer pyramids to multilayer blocks by catalyst-assisted thermal evaporation. *J Mater Sci* 53:8098–8107. <https://doi.org/10.1007/s10853-018-2103-0>

- [28] Zheng J, Yan X, Lu Z et al (2017) High-mobility multilayered MoS₂ flakes with low contact resistance grown by chemical vapor deposition. *Adv Mater* 29:2–7. <https://doi.org/10.1002/adma.201604540>
- [29] Shearer MJ, Samad L, Zhang Y et al (2017) Complex and noncentrosymmetric stacking of layered metal dichalcogenide materials created by screw dislocations. *J Am Chem Soc* 139:3496–3504. <https://doi.org/10.1021/jacs.6b12559>
- [30] Macchione MA, Mendoza-Cruz R, Bazan-Diaz L et al (2020) Electron microscopy study of the carbon-induced 2H-3R-1T phase transition of MoS₂. *New J Chem* 44:1190–1193. <https://doi.org/10.1039/c9nj03850g>
- [31] Cortés N, Rosales L, Orellana PA et al (2018) Stacking change in MoS₂ bilayers induced by interstitial Mo impurities. *Sci Rep* 8:1–8. <https://doi.org/10.1038/s41598-018-20289-1>
- [32] Lee Y-H, Zhang X-Q, Zhang W et al (2012) Synthesis of large-area MoS₂ atomic layers with chemical vapor deposition. *Adv Mater* 24:2320–2325. <https://doi.org/10.1002/adma.201104798>
- [33] Li X-L, Ge J-P, Li Y-D (2004) Atmospheric pressure chemical vapor deposition: an alternative route to large-scale MoS₂ and WS₂ inorganic fullerene-like nanostructures and nanoflowers. *Chem - A Eur J* 10:6163–6171. <https://doi.org/10.1002/chem.200400451>
- [34] Gómez-Rodríguez A, Beltrán-del-Río LM, Herrera-Becerra R (2010) SimulaTEM: multislice simulations for general objects. *Ultramicroscopy* 110:95–104. <https://doi.org/10.1016/j.ultramic.2009.09.010>
- [35] Fan JH, Gao P, Zhang AM et al (2014) Resonance Raman scattering in bulk 2H-MX₂ (M = Mo, W; X = S, Se) and monolayer MoS₂. *J Appl Phys.* <https://doi.org/10.1063/1.4862859>
- [36] Chakraborty B, Matte HSSR, Sood AK, Rao CNR (2013) Layer-dependent resonant Raman scattering of a few layer MoS₂. *J Raman Spectrosc* 44:92–96. <https://doi.org/10.1002/jrs.4147>
- [37] Zheng W, Zhu Y, Li F, Huang F (2018) Raman spectroscopy regulation in van der Waals crystals. *Photonics Res* 6:1101. <https://doi.org/10.1364/prj.6.001101>
- [38] Cross JS, Schrader GL (1995) Low pressure chemical vapor deposition of molybdenum oxides from molybdenum hexacarbonyl and oxygen. *Thin Solid Films* 259:5–13. [https://doi.org/10.1016/0040-6090\(94\)06427-X](https://doi.org/10.1016/0040-6090(94)06427-X)
- [39] Dieterle M, Mestl G (2002) Raman spectroscopy of molybdenum oxides: Part II. Resonance Raman spectroscopic characterization of the molybdenum oxides Mo₄O₁₁ and MoO₂. *Phys Chem Chem Phys* 4:822–826. <https://doi.org/10.1039/b107046k>
- [40] Moura JVB, Silveira JV, da Silva Filho JG et al (2018) Temperature-induced phase transition in h-MoO₃: stability loss mechanism uncovered by Raman spectroscopy and DFT calculations. *Vib Spectrosc* 98:98–104. <https://doi.org/10.1016/j.vibspec.2018.07.008>
- [41] Kondekar NP, Boebinger MG, Woods EV, McDowell MT (2017) In situ XPS investigation of transformations at crystallographically oriented MoS₂ interfaces. *ACS Appl Mater Interfaces* 9:32394–32404. <https://doi.org/10.1021/acsami.7b10230>
- [42] Syari'ati A, Kumar S, Zahid A et al (2019) Photoemission spectroscopy study of structural defects in molybdenum disulfide (MoS₂) grown by chemical vapor deposition (CVD). *Chem Commun* 55:10384–10387. <https://doi.org/10.1039/c9cc01577a>
- [43] Wang QF, Yanzhang RP, Ren XN et al (2016) Two-dimensional molybdenum disulfide and tungsten disulfide interleaved nanowalls constructed on silk cocoon-derived N-doped carbon fibers for hydrogen evolution reaction. *Int J Hydrog Energy* 41:21870–21882. <https://doi.org/10.1016/j.ijhydene.2016.07.257>
- [44] Iranmahboob J, Gardner SD, Toghiani H, Hill DO (2004) XPS study of molybdenum sulfide catalyst exposed to CO and H₂. *J Colloid Interface Sci* 270:123–126. <https://doi.org/10.1016/j.jcis.2003.11.013>
- [45] Wang W, Li L, Tan S et al (2016) Preparation of NiS₂/MoS₂ catalysts by two-step hydrothermal method and their enhanced activity for hydrodeoxygenation of p-cresol. *Fuel* 179:1–9. <https://doi.org/10.1016/j.fuel.2016.03.068>
- [46] Lee YJ, Barrera D, Luo K, Hsu JWP (2012) In situ chemical oxidation of ultrasmall MoOx nanoparticles in suspensions. *J Nanotechnol* 2012:3–8. <https://doi.org/10.1155/2012/195761>
- [47] Rajagopal S, Nataraj D, Khyzhun OY et al (2011) Systematic synthesis and analysis of change in morphology, electronic structure and photoluminescence properties of pyrazine intercalated MoO₃ hybrid nanostructures. *CrystEngComm* 13:2358–2368. <https://doi.org/10.1039/C0CE00303D>
- [48] Huang L, Xu H, Zhang R et al (2013) Synthesis and characterization of g-C₃N₄/MoO₃ photocatalyst with improved visible-light photoactivity. *Appl Surf Sci* 283:25–32. <https://doi.org/10.1016/j.apsusc.2013.05.106>
- [49] Jin S, Bierman MJ, Morin SA (2010) A new twist on nanowire formation: screw-dislocation-driven growth of nanowires and nanotubes. *J Phys Chem Lett* 1:1472–1480. <https://doi.org/10.1021/jz100288z>
- [50] Xia Y, Xiong Y, Lim B, Skrabalak SE (2009) Formkontrolle bei der Synthese von Metallnanokristallen: einfache Chemie, komplexe Physik? *Angew Chemie* 121:62–108. <https://doi.org/10.1002/ange.200802248>

- [51] Dong F, Wu L, Sun Y et al (2011) Efficient synthesis of polymeric g-C₃N₄ layered materials as novel efficient visible light driven photocatalysts. *J Mater Chem* 21:15171. <https://doi.org/10.1039/c1jm12844b>
- [52] Wang H, Robinson JT, Diankov G, Dai H (2010) Nanocrystal growth on graphene with various degrees of oxidation. *Am Chem Soc* 132:3270–3271
- [53] Morin SA, Forticaux A, Bierman MJ, Jin S (2011) Screw dislocation-driven growth of two-dimensional nanoplates. *Nano Lett* 11:4449–4455. <https://doi.org/10.1021/nl202689m>
- [54] Viswanath B, Kundu P, Mukherjee B, Ravishankar N (2008) Predicting the growth of two-dimensional nanostructures. *Nanotechnology* 19:195603. <https://doi.org/10.1088/0957-4484/19/19/195603>
- [55] Sarma PV, Patil PD, Barman PK et al (2016) Controllable growth of few-layer spiral WS₂. *RSC Adv* 6:376–382. <https://doi.org/10.1039/C5RA23020A>
- [56] Gutiérrez HR, Perea-López N, Elías AL et al (2013) Extraordinary room-temperature photoluminescence in triangular WS₂ monolayers. *Nano Lett* 13:3447–3454. <https://doi.org/10.1021/nl3026357>
- [57] van der Zande AM, Huang PY, Chenet DA et al (2013) Grains and grain boundaries in highly crystalline monolayer molybdenum disulphide. *Nat Mater* 12:554–561. <https://doi.org/10.1038/nmat3633>
- [58] Kan M, Wang JY, Li XW et al (2014) Structures and phase transition of a MoS₂ monolayer. *J Phys Chem C* 118:1515–1522. <https://doi.org/10.1021/jp4076355>

Publisher's Note Springer Nature remains neutral with regard to jurisdictional claims in published maps and institutional affiliations.